Electrical Manipulation of Magnetic Anisotropy in a $Fe_{81}Ga_{19}/Pb(Mg_{1/3}Nb_{2/3})O_3$-$Pb(Zr_xTi_{1-x})O_3$ Magnetoelectric Multiferroic Composite

W. Jahjah,[1,2,*] J.-Ph. Jay,[1,†] Y. Le Grand,[1] A. Fessant,[1] A.R.E. Prinsloo,[2] C.J. Sheppard,[2] D.T. Dekadjevi,[1,2] and D. Spenato[1]

[1] *Univ. Brest, Laboratoire d'Optique et de Magnétisme (OPTIMAG), EA 938, 29200 Brest, France*

[2] *Cr Research Group, Department of Physics, University of Johannesburg, PO Box 524, Auckland Park 2006, South Africa*

(Received 1 October 2019; revised manuscript received 13 January 2020; accepted 14 February 2020; published 5 March 2020)

Magnetoelectric composites are an important class of multiferroic materials that are paving the way towards a new generation of multifunctional devices directly integrable into data-storage technology and spintronics. This study focuses on strain-mediated electrical manipulation of magnetization in an extrinsic multiferroic. The composite used includes 5- or 60-nm $Fe_{81}Ga_{19}$ thin films coupled to a piezoelectric (011) $Pb(Mg_{1/3}Nb_{2/3})O_3$-$Pb(Zr_xTi_{1-x})O_3$ (PMN-PZT) material. A magnetization-reversal study reveals a converse magnetoelectric coefficient $\alpha_{CME,max} \approx 2.7 \times 10^{-6}$ s m^{-1} at room temperature. This reported value of α_{CME} is among the highest so far, compared with previous reports on single-phase multiferroics and on composites. An angular dependence of α_{CME} is also shown, arising from the intrinsic magnetic anisotropy of Fe-Ga. The highly efficient magnetoelectric composite Fe-Ga/PMN-PZT demonstrates drastic modifications of the in-plane magnetic anisotropy, with an almost 90° rotation of the preferential anisotropy axis in thinner films under an electric field $E = 10.8$ kV cm^{-1}. Also, the influence of thermal strain on the bilayer's magnetic coercivity is compared with that for a reference Fe-Ga/glass bilayer at cryogenic temperatures. A different evolution is observed as a function of temperature, revealing a thermomechanical influence of the substrate which has not yet been reported in Fe-Ga thin films coupled to a piezoelectric material.

DOI: 10.1103/PhysRevApplied.13.034015

I. INTRODUCTION

Research on magnetoelectric (ME) coupling saw a renaissance [1] when multiferroic (MF) materials were considered in 2005 [2]. MF materials [3] simultaneously show at least two ferroic orderings, such as ferroelectric (FE) and (anti-)ferromagnetic, as well as ferroelastic. There has recently been a frenzy over MF materials in condensed-matter physics due to their novel potential applications, including multifunctional devices such as spintronic devices, ME transducers, actuators, sensors, and multiple-state memories [4–7]. Among the multiferroic orderings, the coexistence of ferroelectricity and ferromagnetism is highly desired, as it allows electric field control of magnetism without the need for magnetic fields, known as the converse ME (CME) effect; the direct ME (DME) effect is magnetic field control of the electric polarization [8]. Multiferroics may thus pave the way to faster, smaller, more energy-efficient data-storage technologies. The CME effect has been observed as an intrinsic effect in some oxide single-phase MF materials [9,10] such as $BiFeO_3$, one of the few multiferroics at room temperature, and thus the most intensively investigated single-phase multiferroic [11–14].

However, most single-phase MF materials possess either a low permittivity or a low permeability at room temperature and thus exhibit weak ME coupling, which hinders their application [15]. In addition, these materials are often complicated to fabricate, potentially leading to electrical-leakage problems due to structural defects and impurities [14,16]. ME composites, on the other hand, also known as extrinsic multiferroics, consist of stacked magnetostrictive and piezoelectric phases and offer a wide range of materials, as well as flexibility in fabrication [17,18]. These composites provide a powerful tool that can be used to achieve a giant ME coupling response at room temperature, when compared with those found for single-phase materials. Great efforts have been made to electrically control the magnetization via three main mechanisms, based on charge carriers [19–21], spin exchange (exchange bias coupling) [22–24],

*walaajahjah@hotmail.com
†jay@univ-brest.fr

 © 2020 American Physical Society

and strain-mediated coupling [20,25–32]. Particularly, the strain-mediated mechanism has been found very appealing for further exploration [16,33]. In strain-mediated composites, ME coupling occurs when, in the case of the CME effect, an applied electric field induces strain in the piezoelectric phase through the direct piezoelectric effect. This strain is transferred to the magnetostrictive phase and, in turn, induces inverse magnetostriction (the Villari effect [34]), which translates into a change in magnetic properties.

To provide the strain, ferroelectrics based on relaxor $PbTiO_3$ (relaxor PT) are widely used for their excellent piezoelectric properties. Rhombohedral $Pb(Mg_{1/3}Nb_{2/3})O_3$-$Pb(Zr_xTi_{1-x})O_3$ (PMN-PZT) single crystals are an example of ternary-system ferroelectrics that provide, near their morphotropic phase boundary, many advantages compared with their binary counterparts $Pb(Mg_{1/3}Nb_{2/3})O_3$-$Pb(Ti)O_3$ (PMN-PT) and PZT-PT or with PZT ceramics [35,36]. They offer comparable piezoelectric coefficients ($d_{33} = 1000$–2000 pC N^{-1}) and electromechanical coupling factors ($k_{33} \geq 0.9$) to binary crystals, while possessing double the coercive-field values, on the order of $E_c = 5$ kV cm^{-1}, higher Curie temperatures ($T_C = 130$–$170\,^{\circ}$C), and higher FE transition temperatures (rhombohedral-to-tetragonal phase transition temperature $T_{RT} = 90$–$160\,^{\circ}$C), significantly expanding the temperature range of usage for high-power applications [36,37]. The notation d_{ij} for the piezoelectric coefficients uses the "j" axis to refer to the working deformation direction under an applied E field along the polarization axis "i," in compliance with the IEEE standards for relaxor-based FE single crystals [38].

Furthermore, it is possible to increase the strain amplitude by cutting and poling the crystal along particular crystallographic directions [39–42]. When relaxor-PT crystals operate in the ⟨110⟩-poled longitudinal-transverse (L-T) mode (32 mode, vibration along ⟨001⟩), they possess very high d_{32} and k_{32} values. Meanwhile, as the crystals are poled and driven through their thickness rather than their length, the electric field required to drive them is much lower than that for the L-L 33 mode [38,43]. Consequently, a large in-plane anisotropic piezostrain can be achieved, with $d_{32} = -1850$ pC N^{-1} and $d_{31} = 599$ pC N^{-1} in the case of (011) PMN-PZT [44–48]. This is a crucial driving mechanism for the observation of large anisotropic ME properties in combination with a magnetostrictive film.

Little focus has been given to electrically controlling the magnetism in such ternary relaxor ferroelectrics. In particular, (011) PMN-PZT single crystals have only recently been used for controlling magnetization through CME coupling in ME composites [49], whereas they have shown a wide range of fresh interesting results for power generation and energy harvesting based on the DME effect [39,41,44–46,48,50–52]. Some of these investigations [39,51] also involved Galfenol or Fe-Ga as the magnetostrictive phase, considering its promising magnetic properties.

Regarding the magnetostrictive phase, Fe-Ga thin films combine remarkable properties such as low hysteresis, large magnetostriction, good tensile strength, machinability, and, more recently, progress in commercially viable methods of processing [53–55]. Although the magnetostrictive properties of Fe-Ga are lower than those of Terfenol-D (a terbium-iron-dysprosium alloy), gallium, when substituted for iron, increases the tetragonal magnetostriction coefficient λ_{100} over tenfold [53]. Another advantage of Fe-Ga alloys is the rare-earth-free composition; the cost is thus reduced compared with the rare-earth-alloy family, which also has another drawback, which is brittleness.

Fe-Ga has been the choice of magnetostrictive material for many studies, which have suggested versatile proposals for the development of multifunctional devices exploiting both the DME [56–58] and the CME effect [9,19,24,59–66]. Among these studies, some have reported a dynamic self-biased effect, also called the remanent CME effect, which is a desirable property that has recently been sought for controlling the magnetization using an electric field in ME devices without the need for the assistance of an external biasing magnetic field [31,49,67–71]. The self-biased CME effect is indeed important for lower-energy-consumption and more compact ME devices.

Nevertheless, the CME coupling has not yet been investigated in a ME composite that brings together two highly performant components in the research that has been done on ME extrinsic multiferroics, such as (011) PMN-PZT ferroelectric single crystals and magnetostrictive polycrystalline $Fe_{81}Ga_{19}$ thin films.

Furthermore, the field of multiferroics covers aspects ranging from technological applications to fundamental research problems. The study of multiferroics is increasingly influencing neighboring research areas, including complex magnetism and ferroelectricity, oxide heterostructures, and interfaces [72]. This is shedding light on the bonding relationship of the two phases in extrinsic MF materials, and showing how a different type of strain such as thermal strain at low temperatures can act on a magnetostrictive material depending on the nature of the substrate. This has never been done before on the Fe-Ga/PMN-PZT system.

In this paper, we report on the magnetoelectric coupling in a $Fe_{81}Ga_{19}$/(011) PMN-PZT composite through a systematic experimental study. For Fe-Ga sample thicknesses $t_{FM} = 5$ and 60 nm, magnetization-reversal loops $M(\mu_0 H)$ (μ_0 being the vacuum permeability) are first presented along the [100] and [0$\bar{1}$1] directions and for only two values of the electric field E in Sec. III A. These measurements are then extended to bipolar E-field cycles to show the evolution of the magnetic properties

in Sec. III B. For more insight into the anisotropy properties, we also present in Sec. III C the azimuthal behavior of Fe-Ga through angular measurements of $M(\mu_0 H)$ for $E = 0$ kV cm^{-1} and $E > 0$ kV cm^{-1}. To quantify the relative magnetization change upon applying an electric field to our ME composite, we report in Sec. III D a CME coupling coefficient $\alpha_{\mathrm{CME}} = \mu_0 \Delta M / \Delta E$ (in s m^{-1}) among the highest reported so far, and compare it with a comprehensive literature recap of reported α_{CME} values. We show as well an angular dependence of α_{CME} that is strongly related to the anisotropy properties of Fe-Ga. Finally, in Sec. III E, we report low-temperature measurements ranging from 10 to 300 K that were carried out in order to explore thermomagnetomechanical effects by comparing the behavior of the temperature-dependent magnetic coercivity of Fe-Ga on two different substrates, amorphous glass and single-crystalline ferroelectric PMN-PZT.

II. EXPERIMENTAL PROCEDURES

Samples consisting of bilayered ME composites are prepared by depositing magnetostrictive Fe-Ga thin films onto piezoelectric (011) PMN-PZT, using radio-frequency magnetron sputtering. PMN-PZT rhombohedral single crystals grown by solid-state crystal growth are commercially available as "CPSC160-95" from Ceracomp Co. Ltd., Korea [73]. Figure 1(a) shows a schematic drawing of a ME composite consisting of magnetostrictive Fe-Ga and a (011) PMN-PZT slab or beam. The PMN-PZT slabs are (011)-oriented and poled along the thickness, and thus along [011], creating an in-plane anisotropic strain behavior which allows the L-T working mode. This means that the (011) plane undergoes an anisotropic deformation when an electric field is applied parallel to the [011] poling direction. Figure 1(b) presents the unit cell of (011) PMN-PZT along with the corresponding working mode.

As presented in Fig. 1(b), poling the crystal along the nonpolar direction [011] creates a macrosymmetric multidomain structure [39,74]. Such an engineered domain state is more stable than the single-domain state and offers an almost hysteresis-free strain-E behavior, because the two dipole orientations [$\bar{1}$11] and [111] are energetically equivalent and are equally populated under the [011] poling. When the (011)-oriented crystal is actuated by E parallel to [011], the two possible polar directions are expected to be inclined close to the direction of E in each domain, which results in an increased rhombohedral lattice distortion and a large piezoelectric response. Such a movement strongly deforms the (011) plane (marked by dashed blue lines): it induces simultaneously a strong compressive strain along the [100] direction (d_{32}) and a tensile strain along the [0$\bar{1}$1] direction (d_{31}) [30]. This results in different signs and magnitudes of the planar piezoelectric coefficients, i.e., $d_{32} = -1850$ pC N^{-1} and $d_{31} = 599$ pC N^{-1}. Therefore the (011)-oriented PMN-PZT single crystal displays large anisotropic piezoelectric properties, with $|d_{32}| \approx 3d_{31}$.

Initially, the PMN-PZT beams, with dimensions $7 \times 5 \times 0.3$ mm^3 ($L \times W \times T$), are cleaned with ethanol and acetone. A $Fe_{81}Ga_{19}$ polycrystalline target with a diameter of 3 inches is used in an Oerlikon Leybold Univex 350 sputtering system. The base pressure prior to the film deposition is typically 10^{-7} mbar. $Fe_{81}Ga_{19}$ thin films are deposited onto the PMN-PZT beams at room temperature using 100 W of deposition power and about 10 sccm argon pressure. The FM Fe-Ga thicknesses are $t_{\mathrm{FM}} = 5$ and

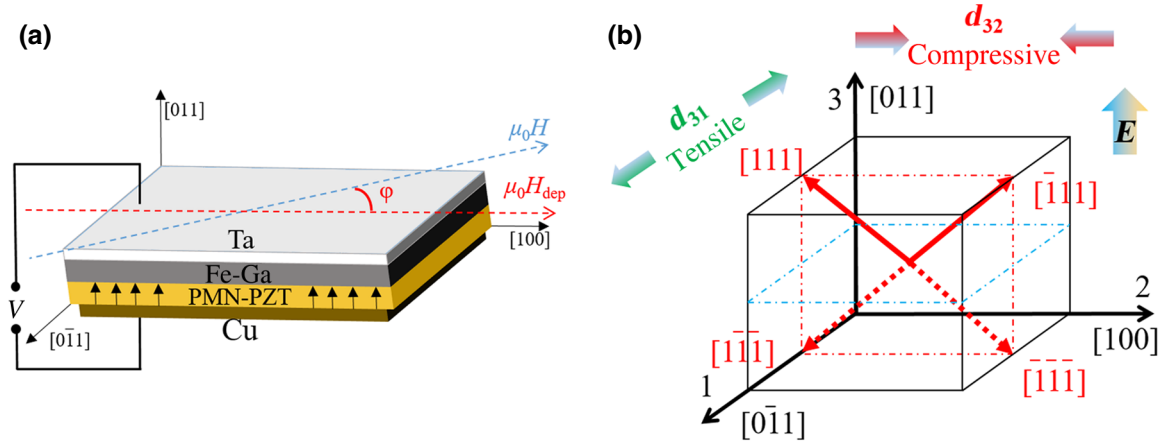

FIG. 1. (a) Schematic drawing of a ME composite consisting of magnetostrictive Fe-Ga and a (011)-oriented PMN-PZT beam or slab. The configuration of the measurement is also indicated using the angle φ between the applied magnetic field $\mu_0 H$ (dashed blue axis) and the deposition field $\mu_0 H_{\mathrm{dep}}$ (dashed red axis along the [100] length of the beam). Black arrows inside the PMN-PZT layer represent the positive electric field direction. The drawing is not to scale. (b) Sketch of the polarization vectors of the rhombohedral PMN-PZT unit cell in the (011)-oriented case. Also presented are the d_{31} and d_{32} modes of strain, the direction of the poling electric field E along [011], and its plane (dashed blue square).

60 nm. The stack is capped *in situ* with a 10-nm-thick Ta layer to protect the Fe-Ga layer against oxidation. The growth is carried out under an in-plane magnetic field $\mu_0 H_{\text{dep}} \sim 30$ mT (300 Oe) along the beam length, i.e., the [100] direction [Fig. 1(a)], in order to favor a preferential magnetic anisotropy direction. Other samples of Ta/Fe-Ga with $t_{\text{FM}} = 5$ and 60 nm are also deposited on glass substrates (Schott D 263 TM [75]), which serve as reference samples.

For an electrical study, metallic electrodes must be available on both sides of the bilayered ME composite. The 10-nm-thick Ta layer serves as a top electrode. For the bottom electrode, the samples are turned over and a 200-nm-thick Cu layer is deposited onto the bottom surface of the PMN-PZT beam using a mask of slightly smaller dimensions (6.5×4.5 mm^2) ($L \times W$) than the PMN-PZT beam to avoid any short-circuit contact along the lateral edges with the Fe-Ga. The final layered structure of our samples is Ta(10 nm)/Fe-Ga(t_{FM})/PMN-PZT(0.3 mm)/Cu(200 nm), as shown in Fig. 1(a).

Static magnetic measurements are performed to probe magnetization reversal with a commercial Evico MOKE (magneto-optical Kerr effect) microscope [76]. An additional setup within the MOKE apparatus is devised to enable the application of an electric field across the sample thickness, thus allowing magnetic measurements to be performed under an applied static electric field [Fig. 1(a)]. The as-deposited samples of Ta(10 nm)/Fe-Ga(t_{FM})/PMN-PZT(0.3 mm)/Cu(200 nm) are held on a support inside the electromagnet. The support base contains a bottom electrode that contacts the bottom Cu layer, and the top Ta layer is in contact with a thin brass needle tip that serves as the top electrode. Both electrodes are wired to a dc power supply (up to 300 V), and an ammeter together with a 10 MΩ protecting resistor are series-wound in the circuit to monitor the current during all the measurements.

Furthermore, the temperature dependence of the coercive field is obtained from the $M(\mu_0 H)$ measurement using a Cryogenic cryogen-free physical-property measurement platform with a vibrating sample magnetometer (VSM) insert [77]. The magnet is initially demagnetized, after which the sample is cooled in zero applied magnetic field to the desired temperature. The value of $M(\mu_0 H)$ is then measured using the low-magnetic-field option of the Cryogenic system.

III. RESULTS AND DISCUSSION

A. Electrical tuning of the magnetization reversal

Electric field control of the magnetization is carried out using the MOKE microscope, which supports an additional *in situ* setup to enable the application of an electric field across the sample thickness. A field E pointing from the PMN-PZT to the Fe-Ga film is defined as a positive

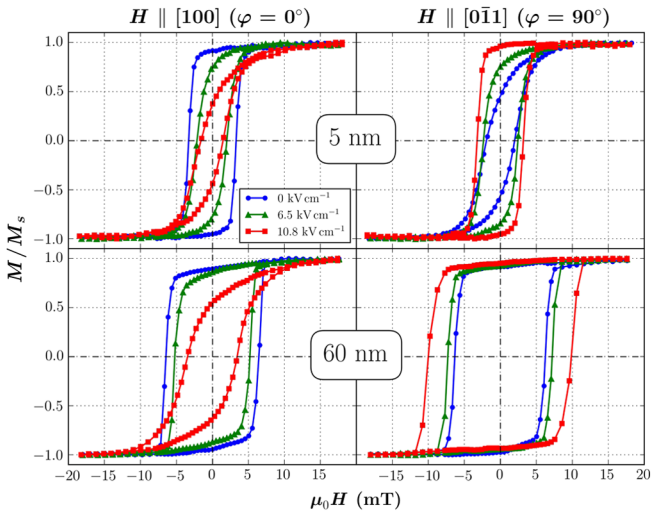

FIG. 2. Hysteresis loops of the normalized magnetization reversal of Ta(10 nm)/Fe-Ga($t_{\text{FM}} = 5$ or 60 nm)/PMN-PZT(0.3 mm)/Cu(200 nm), measured in-plane with the magnetic field $\mu_0 H$ parallel to [100] ($\varphi = 0°$, i.e., along the deposition-field axis $\mu_0 H_{\text{dep}}$) and [0$\bar{1}$1] ($\varphi = 90°$), under three values of electric field $E = 0$, 6.5, and 10.8 kV cm^{-1}.

E (Fig. 1). Routinely, magnetization hysteresis loops are measured along the [100] direction ($\varphi = 0°$) and the [0$\bar{1}$1] direction ($\varphi = 90°$) under different values of the applied electric field E, namely 0, 6.5, and 10 kV cm^{-1}, as presented in Fig. 2. We characterize these loops using the quantity $\mu_0 H_c$ as the coercive field and M_r^n as the remanent magnetization normalized to the saturation magnetization, which is equivalent to the squareness (i.e., $M_r^n = M_r/M_s$).

Under no applied E, the $M(\mu_0 H)$ loops for the 5-nm-thick Fe-Ga sample show an angular dependence when $\mu_0 H_c$ and M_r^n are compared for the two angles $\varphi = 0°$ and 90°. For the 60-nm-thick sample, the $M(\mu_0 H)$ loops show a much less significant angular dependence; $\mu_0 H_c$ and M_r^n show very close values for the two angles. The measured values of $\mu_0 H_c$ and M_r^n are typical of those observed for Fe-Ga thin films [55].

For both $t_{\text{FM}} = 5$ and $t_{\text{FM}} = 60$ nm, the $\mu_0 H_c$ and M_r^n values along [100] decrease when E increases, making the cycles more slanted than square. An easy magnetic anisotropy axis along [100] clearly becomes a harder axis under the application of E. The situation changes when we look at the [0$\bar{1}$1] direction, where the $\mu_0 H_c$ and M_r^n values increase when E increases, and the cycles become more square than slanted. In this case a hard anisotropy axis along [0$\bar{1}$1], especially for the 5-nm-thick sample, becomes an easier axis. These converse reversal behaviors are tightly related to the anisotropic strain in the (011) PMN-PZT induced by E: simultaneously, a strong in-plane compressive strain along [100] (d_{32}) weakens the easy character of the anisotropy and a tensile strain along [0$\bar{1}$1] (d_{31}) weakens its hard character.

The E-field dependence of the $M(\mu_0 H)$ loops along [100] and [0$\bar{1}$1] thus suggests a first sign of switching of a magnetic anisotropy easy axis. Such an axis, when aligned along $\mu_0 H_{\rm dep}$, will tend to align under E in the direction of the tensile stress for a positive magnetostriction λ, i.e., the [0$\bar{1}$1] direction. Hence, the total energy is minimized, including the magnetoelastic term $E_{\rm me} = -(3/2)\lambda\sigma\cos^2\theta$ [34], where σ is the applied stress and θ is the angle between the magnetization and stress.

In Sec. III C, we provide azimuthal measurements in order to provide more insight into the behavior of the anisotropy of the samples.

B. Bipolar E-field measurements

The strain-mediated electric control of magnetization can be extended to a bipolar measurement cycle in which the electric field is swept through positive and negative values. We perform such cycling as follows: $E = +10.8$ kV cm$^{-1} \rightarrow 0$ kV cm$^{-1} \rightarrow -10.8$ kV cm$^{-1} \rightarrow 0$ kV cm^{-1} and finally back to the initial $+10.8$ kV cm^{-1}, with a 1.6 kV cm^{-1} step size. In a strain-mediated FM-FE two-phase system, the bipolar-E-field-controlled magnetization generally exhibits a butterfly-shaped behavior, and an understanding of it has been well established in terms of the piezostrain in the FE substrate transferred to the FM layer [29,78–81].

In reports on the CME effect, it is common to probe the bipolar-E-field tuning of the magnetic moment with $M(E)$ loops, under a constant static magnetic bias field $\mu_0 H$, and to quantify the relative change of M [26,28,30,79,82,83]. Another way of probing the electrically induced change in magnetization would be to extract M_r^n from $M(\mu_0 H)$ as a function of the E loops [30,84] (see the Supplemental Material of Ref. [30]), such as the ones in Fig. 2. In the following, we quantify the relative change of M_r^n extracted from $M(\mu_0 H)$ loops with incremented E values as $\Delta M_r^n/M_r^n(0) = [M_r^n(E_{\rm max}) - M_r^n(0)]/M_r^n(0)$.

We can see in Fig. 3 some nonlinear cycles representing the evolution of $\mu_0 H_c$ and M_r^n as a function of E along both the [100] and the [0$\bar{1}$1] direction. As mentioned earlier in Sec. II, the magnetic bipolar loops in Fig. 3 agree well with a low-hysteresis behavior of the (011) PMN-PZT piezostrain, an almost reversible tuning of the magnetization with positive and negative E, and, most importantly, a remarkable modification of the magnetic properties. For instance, looking at the 5-nm-thick sample, we see that $M_r^n(E)$ along [100] undergoes a relative decrease $\Delta M_r^n/M_r^n(0) \approx 72\%$ upon applying $E_{\rm max} = 10.8$ kV cm^{-1}. Such a relative decrease in magnetization has been previously observed in $Co_{40}Fe_{40}B_{20}$(20 nm)/(011)PMN-PT [30] and in Fe-Al(10 nm)/PIN-PMN-PT [82].

In the case of the 60-nm-thick sample, $\Delta M_r^n/M_r^n(0)$ is reduced to approximately 33%. This decrease with thickness can be associated with a reduced magnetoelastic

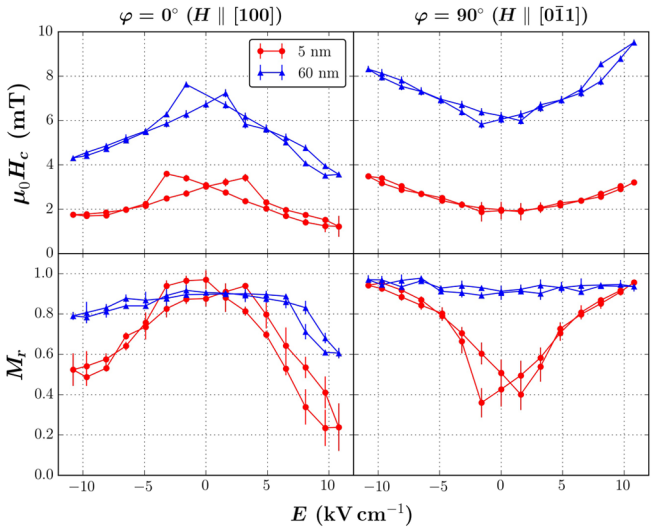

FIG. 3. Electric field control of the coercive field $\mu_0 H_c$ (top row) and the remanent magnetization normalized to the saturation magnetization M_r^n (bottom row) along the two directions [100] (left column) and [0$\bar{1}$1] (right column) for the Ta(10 nm)/Fe-Ga($t_{\rm FM} = 5$ or 60 nm)/PMN-PZT (0.3 mm)/Cu(200 nm) samples. The lines are guides to the eye.

coefficient for Fe-Ga films with increasing thickness, as we have shown in our previous study [55]. Although the piezostrain in the (011) PMN-PZT is strong enough to influence the thin Fe-Ga film, and the direct bonding of the two materials (using the sputtering technique) is among the best techniques for maximum strain transfer, the magnetostriction of the FM phase is an important factor that drives the strain-mediated control of magnetization.

The relative change $\Delta M_r^n/M_r^n(0)$ along [0$\bar{1}$1] follows the opposite trend. $M_r^n(E)$ increases by $\Delta M_r^n/M_r^n(0) \approx 80\%$ when $E = 10.8$ kV cm^{-1} is applied to the 5-nm-thick sample. $M_r^n(E)$ is practically unchanged for the 60-nm-thick sample, which is in agreement with the $M(\mu_0 H)$ results in Fig. 2.

We also note that the electric fields corresponding to the maximum (minimum) $M_r^n(E)$ along [100] ([0$\bar{1}$1]) in Fig. 3 are $\approx \pm 2$ kV cm^{-1}, which are smaller than the coercive field of PMN-PZT, $E_c = 4$ kV cm^{-1}. This has been previously observed in similar ME composites [26]. In the ideal case, a ferroelectric P-E or S-E loop is symmetrical, and so the positive and negative E_c's are equal and correspond to FE-domain switching. Experimentally, the E_c value is not an absolute threshold for FE-domain switching, which may start at E values smaller than E_c. These FE properties may be affected by many factors that shape a ferroelectric P-E or S-E loop, including the thickness of the sample, the presence of charged defects, mechanical stresses, preparation conditions, thermal treatment [85], and relaxation effects in switching FE domains [30].

In addition, Fig. 3 shows an asymmetry in the $M_r^n(E)$ and $\mu_0 H_c(E)$ curves when we look at the highest $E =$

± 10.8 kV cm^{-1}, most noticeably for the $M_r^n(E)$ curves along [100]. This asymmetry may arise from the aforementioned factors, and has been observed previously in magnetoelectric composites [20,26,28,82–84]. Small remanent strain states may be responsible for this asymmetry [84]. It is also presumed that an internal field in the PMN-PZT may be generated, originating from different kinds of defects (e.g., structure, fatigue, or relaxation) in the FE substrate [29,81,86–90].

C. Magnetic azimuthal evolution under *E*

The above results on the electric field control of magnetization are so far presented for the two characteristic directions [100] ($\varphi = 0°$) and [0$\bar{1}$1] ($\varphi = 90°$) of (011) PMN-PZT. In fact, depending on the thickness, Fe-Ga exhibits a considerable angular dependence of its magnetic properties, as shown in Fig. 2. It would be of interest to study this azimuthal dependence to further understand the configuration of the anisotropy by rotating the sample in its plane through an angle φ with respect to $\mu_0 H_{dep}$. In-plane magnetization-reversal measurements are performed every 10°. The azimuthal evolution of $\mu_0 H_c$ and M_r^n as a function of E is reported for all samples in Fig. 4.

Under $E = 0$ kV cm^{-1}, the 5-nm-thick sample shows two maxima of $\mu_0 H_c$ and M_r^n lying along [100], at $\varphi = 0°$ and $\varphi = 180°$. The axis carrying these maxima will be referred to as the "maxima axis", and in this case lies along the direction of $\mu_0 H_{dep}$. Two smaller local maxima of $\mu_0 H_c$ also appear, at $\varphi = 90°$ and $\varphi = 270°$. These local maxima appear as small bumps in the angular representation, and correspond to higher $\mu_0 H_c$ values relative to smaller values or local minima at nearby angles which are not well defined. The angular dependence of $\mu_0 H_c$ indicates a cubic component of the magnetic anisotropy. This has already been observed in our previous work, which revealed a magnetic anisotropy with a predominant in-plane cubic component in thin (5 nm) Fe-Ga films deposited on a glass substrate [55].

Applying an electric field $E = 6.5$ kV cm^{-1} rotates the maxima axis by almost 70°, and a stronger field $E = 10.8$ kV cm^{-1} rotates it further towards the [0$\bar{1}$1] direction by 80°. In fact, applying $E = 10.8$ kV cm^{-1} also changes the azimuthal shape of $\mu_0 H_c$ and M_r^n, which is typical of a uniaxial anisotropy (i.e., two $\mu_0 H_c$ maxima at $\varphi = 80°$ and $\varphi = 260°$, two M_r^n maxima at $\varphi = 90°$ and $\varphi = 270°$, and two minima at $\varphi = 0°$ and $\varphi = 180°$). This amount of rotation of the maxima axis is higher than the reported 55° value for Fe-Al(10 nm)/PIN-PMN-PT under

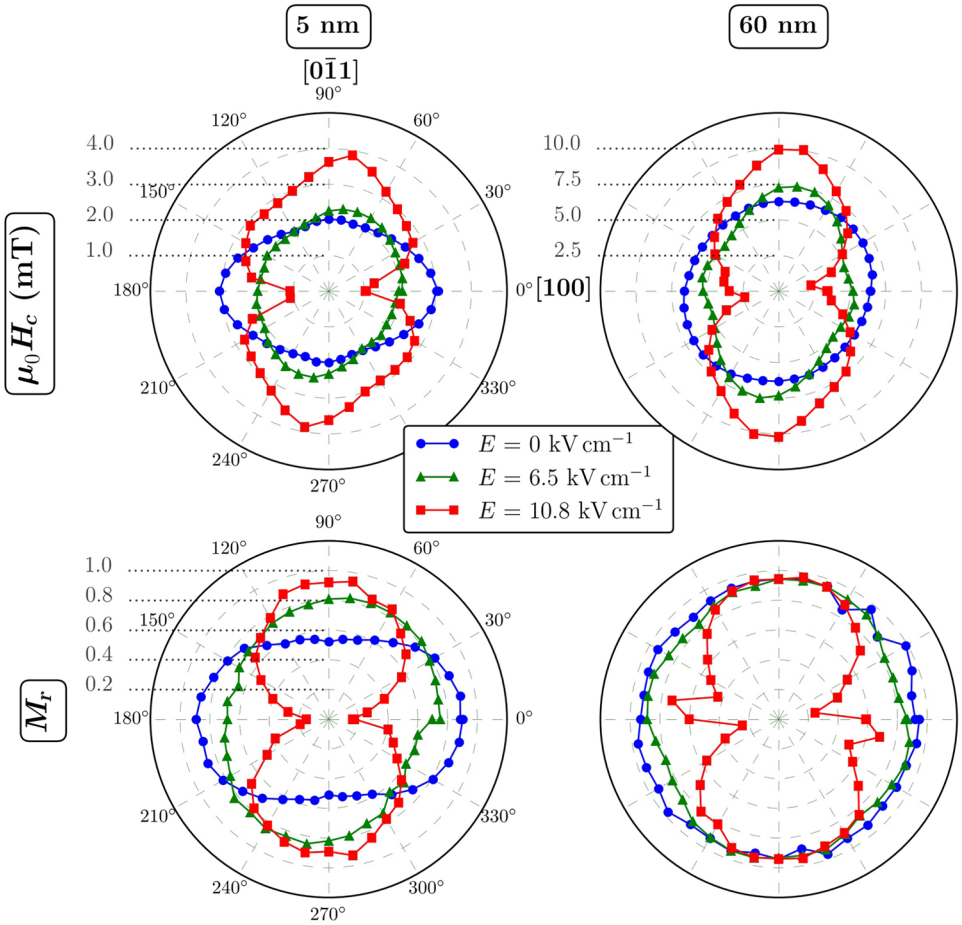

FIG. 4. Azimuthal evolution of the coercive field $\mu_0 H_c$ (first row) and the remanent magnetization normalized to the saturation magnetization M_r^n (second row) extracted from $M(\mu_0 H)$-φ loops. The external magnetic field $\mu_0 H$ is applied at a varying angle φ to the Ta(10 nm)/Fe-Ga($t_{FM} = 5$ or 60 nm)/PMN-PZT(0.3 mm)/Cu(200 nm) samples under three values of the electric field $E = 0$, 6.5, and 10.8 kV cm^{-1}. $\mu_0 H_{dep}$ is applied along [100] ($\varphi = 0°$).

$E = 10$–$12\ \mathrm{kV\,cm^{-1}}$ [82]. It is worth noting that the $\mu_0 H_c$ maxima have higher values $\mu_0 H_{c,\max} = 4$ mT under the highest $E = 10.8\ \mathrm{kV\,cm^{-1}}$ than the maxima $\mu_0 H_{c,\max} = 3$ mT under no applied E. The same remark can be made for the 60-nm-thick sample [30].

Under no applied E, the situation is different for the 60-nm-thick sample: the angular dependence of $\mu_0 H_c$ is quasicircular, revealing a random magnetic anisotropy dispersion [91,92]. This was also observed in our previous paper [55], in which the cubic component of the 5-nm-thick films faded away, but did not vanish, to a more random anisotropy dispersion with increasing thicknesses (greater than or equal to 20 nm). This behavior was attributed to a predominant texture in thinner films, which, in thicker films, is replaced by a nonpreferential polycrystalline arrangement. Cullen *et al.* [91] suggested that competition between coherent and randomly oriented local anisotropies leads to zero or very small net anisotropy in Fe-Ga thin films with almost the same composition (approximately 20% Ga content). In a recent study [92], magnetic-domain-structure observations in Fe-Ga/MgO thin films evidenced this competition between the contributions of coherent cubic anisotropy and random anisotropy.

Under the highest field, $E = 10.8\ \mathrm{kV\,cm^{-1}}$, two maxima of $\mu_0 H_c$ and M_r^n appear at $\varphi \sim 80°$ and $\varphi \sim 260°$ and are accompanied by the development of two local maxima of M_r^n close to $\varphi \sim 0°$ and $\varphi \sim 180°$. It is clear that the random-anisotropy character vanishes, leaving the coexistence of the coherent cubic and uniaxial components under the strain. Under a field $E = 6.5\ \mathrm{kV\,cm^{-1}}$, an intermediate behavior is observed.

D. Magnetoelectric coefficient α_{CME}

To quantify the electric-field-induced variation of the magnetic properties, it is convenient to introduce the converse magnetoelectric coupling coefficient α_{CME} (expressed in $\mathrm{s\,m^{-1}}$), which represents the variation of the magnetization under an applied electric field.

Several methods may be used to calculate α_{CME}. The first one (method *a*) is to consider α_{CME} as the slope (first derivative) of a $M(E)$ loop, i.e., to directly measure the magnetization change as a function of a changing electric field, either under a constant static magnetic bias field $\mu_0 H$ [8,25,26,30,49,82,93] or by saturating the FM film with $\mu_0 H$ and then removing that field [83]. In another method (method *b*), α_{CME} is determined by computing the magnetization from magnetoresistance-loop measurements in a spin-valve device [94]. In our case, an alternative method (method *c*) consists of calculating α_{CME} using the following equation [27,28]:

$$\alpha_{\mathrm{CME}}(\mu_0 H) = \mu_0 \frac{\Delta M_{E_0}(\mu_0 H)}{\Delta E} = \mu_0 \frac{M_{E=E_0}(\mu_0 H) - M_{E=0}(\mu_0 H)}{E_0},$$

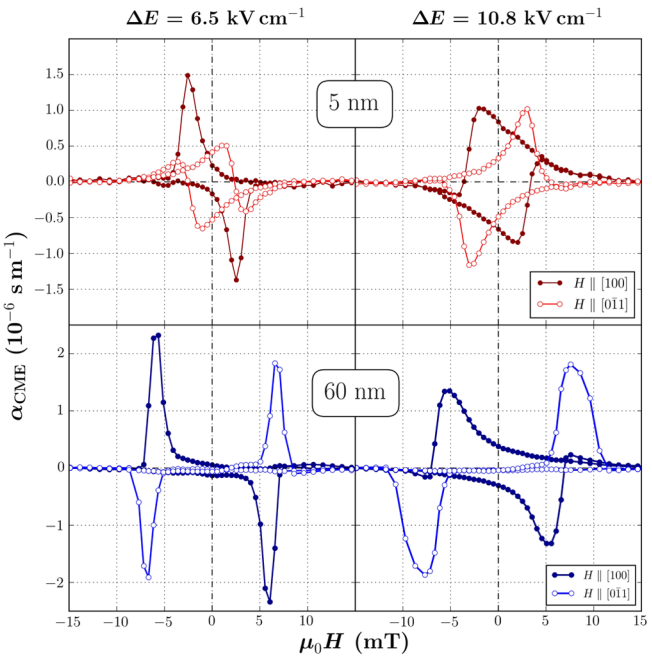

FIG. 5. Converse magnetoelectric coupling coefficient α_{CME} calculated from the $M(\mu_0 H)$ data in Fig. 2 for the Ta(10 nm)/Fe-Ga($t_{\mathrm{FM}} = 5$ or 60 nm)/PMN-PZT(0.3 mm)/Cu(200 nm) samples, under $\Delta E = 6.5$ and $10.8\ \mathrm{kV\,cm^{-1}}$.

with $E_0 = 6.5$ or $10.8\ \mathrm{kV\,cm^{-1}}$. This relative change in magnetization under an applied electric field E is directly computed from the $M(\mu_0 H)$ loops presented in Fig. 2.

The Fe-Ga thin films in this study have a saturation magnetization $\mu_0 M_s = 1.15$ T [55]; we can thus deduce the α_{CME} values in $\mathrm{s\,m^{-1}}$, as shown in Fig. 5, along the two characteristic directions [100] and $[0\bar{1}1]$ of (011) PMN-PZT.

The results reveal a maximum $\alpha_{\mathrm{CME}} = 2.4 \times 10^{-6}\ \mathrm{s\,m^{-1}}$ for the 60-nm-thick sample along [100]. This value is in fact obtained for a lower $\Delta E = 6.5\ \mathrm{kV\,cm^{-1}}$, and for magnetic-bias-field values near $\mu_0 H_c$. Also, for the 5-nm-thick sample, a higher $\alpha_{\mathrm{CME}} = 1.5 \times 10^{-6}\ \mathrm{s\,m^{-1}}$ is obtained along [100] than along $[0\bar{1}1]$. These results are correlated with the fact that the magnetization-reversal loops in Fig. 2 are more significantly modified along [100] than along $[0\bar{1}1]$ under $E = 6.5\ \mathrm{kV\,cm^{-1}}$.

Besides, it is interesting to see nonzero α_{CME} values at zero bias field $\mu_0 H = 0$, especially for the 5-nm-thick sample: $\alpha_{\mathrm{CME}} \sim 0.7 \times 10^{-6}\ \mathrm{s\,m^{-1}}$ for $H \parallel [100]$ and $\Delta E = 10.8\ \mathrm{kV\,cm^{-1}}$. These values correspond to a remanent magnetoelectric coupling at zero bias field $\mu_0 H$, which is related to the hysteretic magnetic behavior and the strong remanent magnetization [49,71]. This is truly encouraging for the potential application of the self-biased dynamic CME effect in Fe-Ga/PMN-PZT; this effect is revealed in measurements that assess the magnetization change under an alternating electric field superimposed on

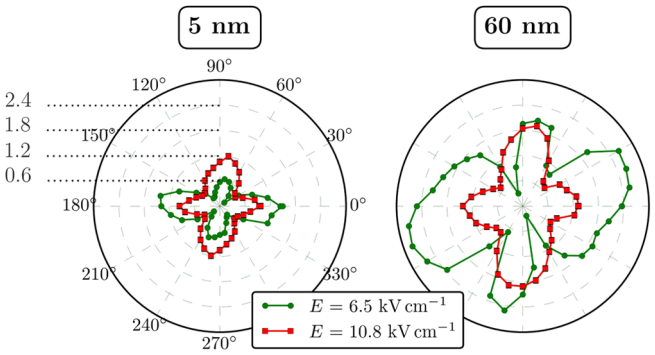

FIG. 6. Azimuthal evolution of the maximum of the converse magnetoelectric coupling coefficient $\alpha_{\mathrm{CME,max}}$ as calculated in Fig. 5, extracted from $M(\mu_0 H)$-φ azimuthal data for the Ta(10 nm)/Fe-Ga($t_{\mathrm{FM}} = 5$ or 60 nm)/PMN-PZT(0.3 mm)/Cu(200 nm) samples, under $\Delta E = 6.5$ and 10.8 kV cm^{-1}.

a dc magnetic bias field $\mu_0 H$ (yielding a nonzero remanent CME effect at $\mu_0 H = 0$) [31,67–69].

Furthermore, as we perform the azimuthal measurements shown in Fig. 4 to assess the angular dependence of $\mu_0 H_c$ and M_r^n, this leads us to believe that the CME behavior may be based specifically on certain nontrivial orientations φ rather than only the crystallographic [100] and [0$\bar{1}$1] directions. We thus calculate the angular dependence of α_{CME} by applying the same method as that used in Fig. 5 to the $M(\mu_0 H)$-φ loops used in Fig. 4. The maximum value of α_{CME} is plotted as $\alpha_{\mathrm{CME,max}}$ for each angle φ in Fig. 6.

The angular behavior of $\alpha_{\mathrm{CME,max}}$ shows peculiar symmetric shapes, especially under $\Delta E = 6.5$ kV cm^{-1}. This confirms that the α_{CME} method (*c*) considered depends exclusively on the characteristics of the measured $M(\mu_0 H)$-φ loops related to both $\mu_0 H_c$ and M_r^n. We remind the reader that these values of $\alpha_{\mathrm{CME,max}}$ correspond to peak values of α_{CME} for bias-field values $\mu_0 H$ close to $\mu_0 H_c$ (Fig. 5), and not to α_{CME} taken at zero bias field $\mu_0 H$. A zero bias field $\mu_0 H$ corresponds exclusively to the $M_r^n(E)$ case that was explored in Fig. 3.

By looking at the 60-nm-thick sample, we can deduce an even higher value than the ones obtained at $\varphi = 0°$ and 90°, of $\alpha_{\mathrm{CME,max}} \approx 2.7 \times 10^{-6}$ s m^{-1} at $\varphi = 30°$ and $\varphi = 210°$. Such results confirm the anisotropic nature of the CME effect in anisotropic Fe-Ga thin films. A stronger electric field $E = 10.8$ kV cm^{-1} brings about a more uniform fourfold symmetry of $\alpha_{\mathrm{CME,max}}$ for all samples. Two maximum values $\alpha_{\mathrm{CME,max}} \approx 1.8 \times 10^{-6}$ s m^{-1} are found around $\varphi = 90°$ and $\varphi = 270°$, and two lower maxima around $\varphi = 0°$ and $\varphi = 180°$. This behavior is similar to the stronger modification of $\mu_0 H_c$ by E along [0$\bar{1}$1].

To our knowledge, this value of α_{CME} obtained at room temperature is several orders of magnitude higher than the values for single-phase multiferroics reported in the literature on the CME effect, as well as higher than or comparable to reported values for other composite multiferroics. In Table I, a comprehensive list is given of the reported values of the CME effect.

It is important to note that such a high achievable α_{CME} is obtained in a unipolar measurement of $|\Delta E| = |0 - 6.5|$ kV cm^{-1} with a non-180° polarization switching of the ferroelectric domains in (011) PMN-PZT (as explored in the bipolar measurements shown in Fig. 3), which is expected to fatigue the FE single crystal, induce relaxation effects, and alter the performance of ME devices [78,87].

TABLE I. Literature recap of values of converse magnetoelectric coupling coefficient α_{CME} (in s m^{-1}) for different magnetoelectric composite materials.

Multiferroic system	α_{CME} (s m^{-1})	T (K)	Ref.
$CoFe_2O_4$(200 nm)/PMN-PT	3.2×10^{-8}[a]	300	[26]
$La_{0.7}Sr_{0.3}MnO_3$(20–50 nm)/PMN-PT	6.0×10^{-8}[a]	330	[25]
$Co_{0.9}Fe_{0.1}$(2.3 nm)/Cu/$Co_{0.9}Fe_{0.1}$(2.5 nm)/$BiFeO_3$	1.0×10^{-7}[b]	300	[94]
$La_{0.67}Sr_{0.33}MnO_3$(40 nm)/$BaTiO_3$	2.3×10^{-7}[a]	157	[8]
YIG(600 nm)/PMN-PZT	3.1×10^{-7}[a]	300	[49]
$La_{0.7}Ca_{0.3}MnO_3$(10 nm)/$BaTiO_3$	5×10^{-7}[c]	20	[27]
Terfenol-D/PZT	7.8×10^{-7}	300	[95]
FeRh(22 nm)/$BaTiO_3$	1.4×10^{-6}[a]	385	[93]
$Fe_{81}Al_{19}$(10 nm)/PIN-PMN-PT	1.6×10^{-6}[a]	300	[82]
$Co_{40}Fe_{40}B_{20}$(20 nm)/PMN-PT	2.0×10^{-6}[a]	300	[30]
$Fe_{81}Ga_{19}$(60 m)/PMN-PZT	**2.7×10^{-6}**[c]	**300**	**This work**
$Fe_{50}Co_{50}$(80 nm)/Ag/PIN-PMN-PT	3.5×10^{-6}[c]	300	[28]
$Co_{40}Fe_{40}B_{20}$(50 nm)/PMN-PT	8.0×10^{-6}[a]	300	[83]

[a]Method *a* for computing α_{CME}.
[b]Method *b*.
[c]Method *c*.

Therefore, electric field control of the magnetization in the unipolar case should be preferred for, for example, high-speed applications of strain-mediated magnetoelectric random access memories in similar structures [5]. Another key point is that our value of the coupling α_{CME} is obtained in a static nonresonant mode of measurement. This is not only promising for realizing nonresonant ME devices, but also appealing for performing dynamic measurements, which are expected to boost this value of α_{CME}; however, such measurements are beyond the scope of this study.

Thus, the tunable converse ME effect reported here is particularly significant in terms of the strong variation of magnetization reversal. Finally, even though a higher α_{CME} is achieved with the thicker 60-nm Fe-Ga film, it is noteworthy that α_{CME} for the thinner 5-nm film is still high enough compared with the other reported values for thicker films in Table I. The 5-nm film offers also the advantage of a nonzero remanent α_{CME}, i.e., at $\mu_0 H = 0$.

E. Thermomechanical effects

In the previous sections, the magnetoelectric effect is investigated for a Fe-Ga/PMN-PZT composite. A strain in the PMN-PZT substrate driven by an applied electric field indeed manipulates the magnetization state and anisotropy of the Fe-Ga.

Another parameter that may modify the internal strain and stress—and, thus, the magnetic anisotropy through inverse magnetostriction—is the temperature, through thermal expansion. Temperature is an important factor for the stability of ME devices operating in complex environments. The ME effect has only rarely been reported at low temperatures for power generation (using the DME effect) [96,97]. However, measuring the temperature-dependent ME effect in our samples is beyond the scope of this study. Instead, we aim to examine the potential influence of the thermal expansion of the PMN-PZT substrate on the magnetic properties of the Fe-Ga as a function of temperature, in order to gain more insight into how thermal strain can act on a magnetostrictive material deposited on a ferroelectric single crystal.

We perform magnetic and temperature measurements, using a Cryogenic cryogen-free physical-property measurement platform with a VSM insert. The sample is zero-field cooled (ZFC) to the desired temperature (from 300 down to 10 K for example), and then $M(\mu_0 H)$ is measured, from which we can extract the coercive field $\mu_0 H_c$. We note that the results are the same in both the ZFC and the field-cooled mode. We use two different substrates for the purpose of discriminating between the thermal expansion of the FM material and of the substrate, amorphous glass and single-crystalline ferroelectric PMN-PZT. The samples thus consist of Ta(10 nm)/Fe-Ga(t_{FM} = 5 or 60 nm)/PMN-PZT(0.3 mm) and the reference bilayers consist of Ta(10 nm)/Fe-Ga(t_{FM} = 5 or 60 nm)/glass(0.5 mm). The corresponding $M(\mu_0 H)$ loops are presented in Fig. 7 for temperatures of 300 and 10 K.

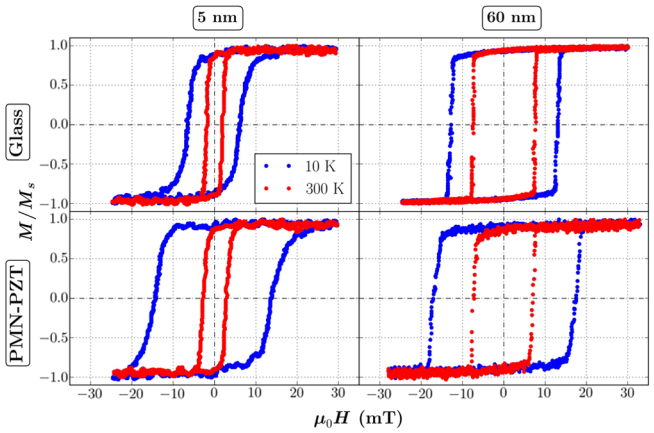

FIG. 7. Hysteresis loops of normalized magnetization reversal at 300 and 10 K for the Ta(10 nm)/Fe-Ga(t_{FM} = 5 or 60 nm)/PMN-PZT(0.3 mm) and Ta(10 nm)/Fe-Ga(t_{FM} = 5 or 60) nm/glass (0.5 mm) samples, measured in-plane with the magnetic field $\mu_0 H$ parallel to [100] ($\varphi = 0°$, i.e., along the axis of the deposition field $\mu_0 H_{dep}$).

The $M(\mu_0 H)$ loops in Fig. 7 show a drastic influence of temperature on the $\mu_0 H_c$ values. The remanence, however, is not affected. For both thicknesses, the $\mu_0 H_c$ values are similar at room temperature (300 K) for both substrates. At 10 K, these values diverge depending on the substrate.

The evolution of $\mu_0 H_c$ as a function of the measuring temperature for the two substrates and the two values of t_{FM} is presented in Fig. 8. $\mu_0 H_c$ typically decreases with

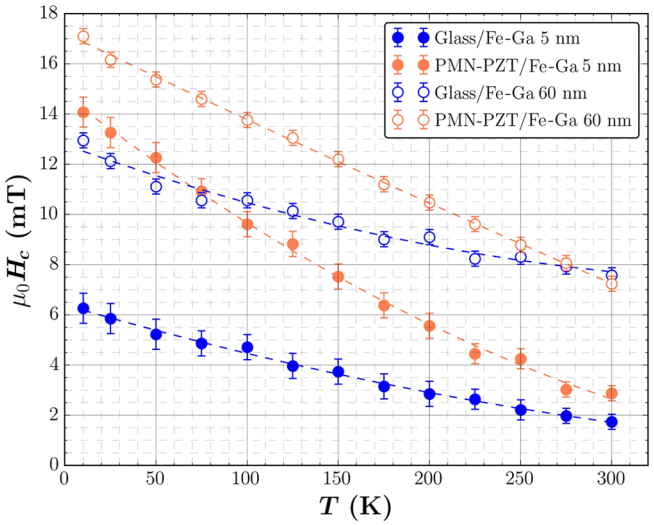

FIG. 8. Temperature-dependent evolution of the coercive field $\mu_0 H_c$ of 5- and 60-nm-thick Fe-Ga samples (filled and empty circles, respectively) deposited onto two different substrates, glass (blue circles) and (011) PMN-PZT (orange circles). The dashed lines are guides to the eye.

increasing temperature, as a result of thermal agitation [13,55]. Nevertheless, comparing the results for one value of t_{FM} of Fe-Ga between the two substrates (blue and orange circles) reveals a clear difference in the slope of the curve of $\Delta(\mu_0 H_c)/\Delta T$. Therefore, below 300 K, the $\mu_0 H_c$ values for one value of t_{FM} for the Fe-Ga gradually diverge when the two substrates are compared. In particular, $\mu_0 H_c$ for the 5-nm-thick sample increases between 300 and 10 K by approximately sixfold on PMN-PZT, whereas on glass it increases threefold. It is also noteworthy that the slope of the $\mu_0 H_c(T)$ curve for $\Delta(\mu_0 H_c)/\Delta T$ is independent of the film thickness; there are almost parallel curves (color-filled and open circles) for the two values of t_{FM} and a single substrate. This has also been shown in our previous work ([55], Fig. 7).

A similar substrate-dependent trend in the evolution of $\mu_0 H_c$ at low temperatures was also observed when comparing exchange-biased Fe-Ga/Ir-Mn bilayers deposited on piezoelectric PVDF for electrical manipulation, and on Si substrates [98].

Consequently, at low temperatures, when Fe-Ga is grown on piezoelectric PMN-PZT, its coercivity responds differently to thermal strain compared with growth on glass. This reveals a combined thermomagnetomechanical effect, which has been previously observed in other systems [98–100]. Such phenomena may be attributed to differences in the elastic properties of glass and PMN-PZT substrates [40,97].

IV. CONCLUSION

In summary, we demonstrate an electrical modulation at room temperature of magnetic properties in an extrinsic multiferroic fabricated by sputtering polycrystalline $Fe_{81}Ga_{19}$ thin films onto (011)-cut and poled PMN-PZT ferroelectric single crystals.

In-plane azimuthal magnetization-reversal measurements enable us to assess, under an applied electric field, the modification of the character of the magnetic anisotropy: the cubic component in thinner films (5 nm) shifts towards a predominant uniaxial component. This shift is accompanied by a 90° rotation of the as-deposited preferential anisotropy axis, and a relative remanent-magnetization change of about 80%. In thicker films (60 nm), the random character of the anisotropy vanishes under E, leaving a coexisting cubic and uniaxial character.

With the assistance of small magnetic fields near the value of $\mu_0 H_c$, an electric field is capable of switching the magnetization state, and we achieve a converse magnetoelectric coupling coefficient $\alpha_{CME} = 2.7 \times 10^{-6}\ \mathrm{s\,m^{-1}}$ at an angle $\varphi = 30°$ between $\mu_0 H$ and the direction of the deposition field $\mu_0 H_{dep}$. This angular dependence of α_{CME} is computed and reported here for a multiferroic. The sizable ME coupling is attributed to many important factors: the high in-plane piezoelectric coefficients of (011) PMN-PZT, the reasonable magnetic properties of Fe-Ga such as the high saturation magnetization. and the high magnetoelastic coefficients. This reported value of α_{CME} is in the range of the highest previously reported values for single-phase multiferroics and similar composites. We also shed light on an azimuthal behavior of α_{CME} driven not only by the anisotropic ferroelectric substrate but also by the anisotropic Fe-Ga.

This ME multiferroic composite promises good results regarding the self-bias effect in a dynamic measurement for achieving a remanent CME effect at zero magnetic bias field. Such highly performant combined materials may increase the pace of progress towards novel multifunctional devices such as microwave devices, where anisotropy is required, and electrically tunable magnetoelectric memories.

We also find that the character of the anisotropy of Fe-Ga appears to be the same at room temperature for two different types of substrate, i.e., amorphous glass and single-crystalline ferroelectric PMN-PZT. However, at low temperatures the mechanical nature of the substrate strongly influences the magnetic behavior. This provides a useful insight into the nature of the bonding between magnetostrictive and piezoelectric materials, and ultimately into the performance of CME composites in complex environments involving cryogenic temperatures.

ACKNOWLEDGMENTS

We wish to acknowledge the support of Region Bretagne (ARED), France, in cofunding W.J.'s Ph.D. This work was also supported by the South African National Research Foundation (Grant No. 80880) and the URC and FRC of the University of Johannesburg, South Africa.

[1] N. A. Spaldin and M. Fiebig, The renaissance of magnetoelectric multiferroics, Science **309**, 391 (2005).
[2] S. Fusil, V. Garcia, A. Barthélémy, and M. Bibes, Magnetoelectric devices for spintronics, Annu. Rev. Mater. Res. **44**, 91 (2014).
[3] W. Eerenstein, N. D. Mathur, and J. F. Scott, Multiferroic and magnetoelectric materials, Nature **442**, 759 (2006).
[4] F. Matsukura, Y. Tokura, and H. Ohno, Control of magnetism by electric fields, Nat. Nanotechnol. **10**, 209 (2015).
[5] J.-M. Hu, Z. Li, L.-Q. Chen, and C.-W. Nan, High-density magnetoresistive random access memory operating at ultralow voltage at room temperature, Nat. Commun. **2**, 1 (2011).
[6] D. Chiba, M. Sawicki, Y. Nishitani, Y. Nakatani, F. Matsukura, and H. Ohno, Magnetization vector manipulation by electric fields, Nature **455**, 515 (2008).
[7] J. T. Heron, M. Trassin, K. Ashraf, M. Gajek, Q. He, S. Y. Yang, D. E. Nikonov, Y.-H. Chu, S. Salahuddin, and

R. Ramesh, Electric-Field-Induced Magnetization Reversal in a Ferromagnet-Multiferroic Heterostructure, Phys. Rev. Lett. **107**, 217202 (2011).

[8] W. Eerenstein, M. Wiora, J. L. Prieto, J. F. Scott, and N. D. Mathur, Giant sharp and persistent converse magnetoelectric effects in multiferroic epitaxial heterostructures, Nat. Mater. **6**, 348 (2007).

[9] T. Zhao, A. Scholl, F. Zavaliche, K. Lee, M. Barry, A. Doran, M. P. Cruz, Y. H. Chu, C. Ederer, N. A. Spaldin, R. R. Das, D. M. Kim, S. H. Baek, C. B. Eom, and R. Ramesh, Electrical control of antiferromagnetic domains in multiferroic BiFeO3 films at room temperature, Nat. Mater. **5**, 823 (2006).

[10] N. Hur, S. Park, P. A. Sharma, J. S. Ahn, S. Guha, and S.-W. Cheong, Electric polarization reversal and memory in a multiferroic material induced by magnetic fields, Nature **429**, 392 (2004).

[11] G. Catalan and J. F. Scott, Physics and applications of bismuth ferrite, Adv. Mater. **21**, 2463 (2009).

[12] T. Hauguel, S. P. Pogossian, D. T. Dekadjevi, D. Spenato, J.-P. Jay, and J. Ben Youssef, Driving mechanism of exchange bias and magnetic anisotropy in multiferroic polycrystalline BiFeO3/permalloy bilayers, J. Appl. Phys. **112**, 093904 (2012).

[13] J. Richy, T. Hauguel, J.-P. Jay, S. P. Pogossian, B. Warot-Fonrose, C. J. Sheppard, J. L. Snyman, A. M. Strydom, J. B. Youssef, A. R. E. Prinsloo, D. Spenato, and D. T. Dekadjevi, Temperature dependence of exchange biased multiferroic $BiFeO_3/Ni_{81}Fe_{19}$ polycrystalline bilayer, J. Phys. Appl. Phys. **51**, 125308 (2018).

[14] W. Jahjah, J.-P. Jay, Y. Le Grand, A. Fessant, J. Richy, C. Marcelot, B. Warot-Fonrose, A. R. E. Prinsloo, C. J. Sheppard, D. T. Dekadjevi, and D. Spenato, Influence of mesoporous or parasitic BiFeO3 structural state on the magnetization reversal in multiferroic $BiFeO_3/Ni_{81}Fe_{19}$ polycrystalline bilayers, J. Appl. Phys. **124**, 235309 (2018).

[15] H. Palneedi, V. Annapureddy, S. Priya, and J. Ryu, Status and perspectives of multiferroic magnetoelectric composite materials and applications, Actuators **5**, 9 (2016).

[16] Y. Wang, J. Hu, Y. Lin, and C.-W. Nan, Multiferroic magnetoelectric composite nanostructures, NPG Asia Mater. **2**, 61 (2010).

[17] G. Srinivasan, Magnetoelectric composites, Annu. Rev. Mater. Res. **40**, 153 (2010).

[18] C.-W. Nan, M. I. Bichurin, S. Dong, D. Viehland, and G. Srinivasan, Multiferroic magnetoelectric composites: Historical perspective, status, and future directions, J. Appl. Phys. **103**, 031101 (2008).

[19] C. A. F. Vaz, Electric field control of magnetism in multiferroic heterostructures, J. Phys.: Condens. Matter **24**, 333201 (2012).

[20] T. Nan *et al.*, Quantification of strain and charge co-mediated magnetoelectric coupling on ultra-thin Permalloy/PMN-PT interface, Sci. Rep. **4**, 3688 (2014).

[21] Z. Zhou, B. M. Howe, M. Liu, T. Nan, X. Chen, K. Mahalingam, N. X. Sun, and G. J. Brown, Interfacial charge-mediated non-volatile magnetoelectric coupling in Co0.3Fe0.7/Ba0.6Sr0.4TiO3/Nb:SrTiO3 multiferroic heterostructures, Sci. Rep. **5**, 7740 (2015).

[22] V. Laukhin, V. Skumryev, X. Martí, D. Hrabovsky, F. Sánchez, M. V. García-Cuenca, C. Ferrater, M. Varela, U. Lüders, J. F. Bobo, and J. Fontcuberta, Electric-Field Control of Exchange Bias in Multiferroic Epitaxial Heterostructures, Phys. Rev. Lett. **97**, 227201 (2006).

[23] Y. Yang, Y. Gong, S. Ma, C. Shen, D. Wang, Q. Cao, Z. Zhong, and Y. Du, Electric-field control of exchange bias field in a $Mn_{50.1}Ni_{39.3}Sn_{10.6}$/piezoelectric laminate, J. Alloys Compd. **619**, 1 (2015).

[24] M. Liu, J. Lou, S. Li, and N. X. Sun, E-field control of exchange bias and deterministic magnetization switching in AFM/FM/FE multiferroic heterostructures, Adv. Funct. Mater. **21**, 2593 (2011).

[25] C. Thiele, K. Dörr, O. Bilani, J. Rödel, and L. Schultz, Influence of strain on the magnetization and magnetoelectric effect in $La_{0.7}A_{0.3}MnO_3$/PMN-PT (001) (A = Sr, Ca), Phys. Rev. B **75**, 054408 (2007).

[26] J. J. Yang, Y. G. Zhao, H. F. Tian, L. B. Luo, H. Y. Zhang, Y. J. He, and H. S. Luo, Electric field manipulation of magnetization at room temperature in multiferroic $CoFe_2O_4/Pb(Mg_{1/3}Nb_{2/3})_{0.7}Ti_{0.3}O_3$ heterostructures, Appl. Phys. Lett. **94**, 212504 (2009).

[27] A. Alberca, C. Munuera, J. Azpeitia, B. Kirby, N. M. Nemes, A. M. Perez-Muñoz, J. Tornos, F. J. Mompean, C. Leon, J. Santamaria, and M. Garcia-Hernandez, Phase separation enhanced magneto-electric coupling in La0.7Ca0.3MnO3/BaTiO3 ultra-thin films, Sci. Rep. **5**, 17926 (2015).

[28] M. Staruch, D. B. Gopman, Y. L. Iunin, R. D. Shull, S. F. Cheng, K. Bussmann, and P. Finkel, Reversible strain control of magnetic anisotropy in magnetoelectric heterostructures at room temperature, Sci. Rep. **6**, 37429 (2016).

[29] T. Wu, A. Bur, K. P. Mohanchandra, K. Wong, K. L. Wang, C. S. Lynch, and G. P. Carman, Giant electric-field-induced reversible and permanent magnetization reorientation on magnetoelectric Ni/(011) $[Pb(Mg_{1/3}Nb_{2/3})O_3](1-x)$–$[PbTiO_3]x$ heterostructure, Appl. Phys. Lett. **98**, 012504 (2011).

[30] S. Zhang, Y. Zhao, X. Xiao, Y. Wu, S. Rizwan, L. Yang, P. Li, J. Wang, M. Zhu, H. Zhang, X. Jin, and X. Han, Giant electrical modulation of magnetization in $Co_{40}Fe_{40}B20/Pb(Mg_{1/3}Nb_{2/3})_{0.7}Ti_{0.3}O_3$(011) heterostructure, Sci. Rep. **4**, 3727 (2015).

[31] C. Yang, P. Li, Y. Wen, A. Yang, D. Wang, F. Zhang, and J. Zhang, Giant converse magnetoelectric effect in PZT/FeCuNbSiB/FeGa/FeCuNbSiB/PZT laminates without magnetic bias field, IEEE Trans. Magn. **51**, 1 (2015).

[32] A. K. Biswas, H. Ahmad, J. Atulasimha, and S. Bandyopadhyay, Experimental demonstration of complete 180° reversal of magnetization in isolated Co nanomagnets on a PMN–PT substrate with voltage generated strain, Nano Lett. **17**, 3478 (2017).

[33] Y. Cheng, B. Peng, Z. Hu, Z. Zhou, and M. Liu, Recent development and status of magnetoelectric materials and devices, Phys. Lett. A **382**, 3018 (2018).

[34] E. Du Trémolet de Lacheisserie, *Magnetostriction: Theory and Applications of Magnetoelasticity* (CRC Press, Boca Raton, 1993).

[35] S. Zhang, S.-M. Lee, D.-H. Kim, H.-Y. Lee, and T. R. Shrout, Electromechanical properties of PMN–PZT piezoelectric single crystals near morphotropic phase boundary compositions, J. Am. Ceram. Soc. **90**, 3859 (2007).

[36] S. Zhang and T. R. Shrout, Relaxor-PT single crystals: Observations and developments, IEEE Trans. Ultrason. Ferroelectr. Freq. Control **57**, 2138 (2010).

[37] T. Richter, S. Denneler, C. Schuh, E. Suvaci, and R. Moos, Textured PMN–PT and PMN–PZT, J. Am. Ceram. Soc. **91**, 929 (2008).

[38] IEEE Standard for Relaxor-Based Single Crystals for Transducer and Actuator Applications. doi:10.1109/IEEESTD.2017.8241013

[39] H. Palneedi, S.-M. Na, G.-T. Hwang, M. Peddigari, K. W. Shin, K. H. Kim, and J. Ryu, Highly tunable magnetoelectric response in dimensional gradient laminate composites of Fe-Ga alloy and $Pb(Mg_{1/3}Nb_{2/3})O_3$–$Pb(Zr, Ti)O_3$ single crystal, J. Alloys Compd. **765**, 764 (2018).

[40] F. Wang, S. W. Or, X. Zhao, and H. Luo, Cryogenic dielectric and piezoelectric activities in rhombohedral $(1-x)Pb(Mg_{1/3}Nb_{2/3})O_{3-x}PbTiO_3$ single crystals with different crystallographic orientations, J. Phys. D: Appl. Phys. **42**, 182001 (2009).

[41] G.-T. Hwang, H. Palneedi, B. M. Jung, S. J. Kwon, M. Peddigari, Y. Min, J.-W. Kim, C.-W. Ahn, J.-J. Choi, B.-D. Hahn, J.-H. Choi, W.-H. Yoon, D.-S. Park, S.-B. Lee, Y. Choe, K.-H. Kim, and J. Ryu, Enhancement of magnetoelectric conversion achieved by optimization of interfacial adhesion layer in laminate composites, ACS Appl. Mater. Interfaces **10**, 32323 (2018).

[42] L. Luo, H. Wang, Y. Tang, X. Zhao, Z. Feng, D. Lin, and H. Luo, Ultrahigh transverse strain and piezoelectric behavior in $(1-x)Pb(Mg_{1-3}Nb_{2-3})O_{3-x}PbTiO_3$ crystals, J. Appl. Phys. **99**, 024104 (2006).

[43] J. Luo and S. Zhang, Advances in the growth and characterization of relaxor-PT-based ferroelectric single crystals, Crystals **4**, 306 (2014).

[44] D. Rajaram Patil, R. C. Kambale, Y. Chai, W.-H. Yoon, D.-Y. Jeong, D.-S. Park, J.-W. Kim, J.-J. Choi, C.-W. Ahn, B.-D. Hahn, S. Zhang, K. Hoon Kim, and J. Ryu, Multiple broadband magnetoelectric response in thickness-controlled Ni/[011] $Pb(Mg_{1/3}Nb_{2/3})O_3$–$Pb(Zr, Ti)O_3$ single crystal/Ni laminates, Appl. Phys. Lett. **103**, 052907 (2013).

[45] R. C. Kambale, W.-H. Yoon, D.-S. Park, J.-J. Choi, C.-W. Ahn, J.-W. Kim, B.-D. Hahn, D.-Y. Jeong, B. Chul Lee, G.-S. Chung, and J. Ryu, Magnetoelectric properties and magnetomechanical energy harvesting from stray vibration and electromagnetic wave by $Pb(Mg_{1/3}Nb_{2/3})O_3$–$Pb(Zr, Ti)O_3$ single crystal/Ni cantilever, J. Appl. Phys. **113**, 204108 (2013).

[46] J. Ryu, J.-E. Kang, Y. Zhou, S.-Y. Choi, W.-H. Yoon, D.-S. Park, J.-J. Choi, B.-D. Hahn, C.-W. Ahn, J.-W. Kim, Y.-D. Kim, S. Priya, S. Y. Lee, S. Jeong, and D.-Y. Jeong, Ubiquitous magneto-mechano-electric generator, Energy Environ. Sci. **8**, 2402 (2015).

[47] H. Palneedi, V. Annapureddy, H.-Y. Lee, J.-J. Choi, S.-Y. Choi, S.-Y. Chung, S.-J. L. Kang, and J. Ryu, Strong and anisotropic magnetoelectricity in composites of magnetostrictive Ni and solid-state grown lead-free piezoelectric BZT–BCT single crystals, J. Asian Ceram. Soc. **5**, 36 (2017).

[48] O. Bilgen, M. Amin Karami, D. J. Inman, and M. I. Friswell, The actuation characterization of cantilevered unimorph beams with single crystal piezoelectric materials, Smart Mater. Struct. **20**, 055024 (2011).

[49] J. Lian, F. Ponchel, N. Tiercelin, Y. Chen, D. Rémiens, T. Lasri, G. Wang, P. Pernod, W. Zhang, and X. Dong, Electric field tuning of magnetism in heterostructure of yttrium iron garnet film/lead magnesium niobate-lead zirconate titanate ceramic, Appl. Phys. Lett. **112**, 162904 (2018).

[50] C.-S. Park, K.-H. Cho, M. A. Arat, J. Evey, and S. Priya, High magnetic field sensitivity in $Pb(Zr, Ti)O_3$–$Pb(Mg_{1/3}Nb_{2/3})O_3$ single crystal/Terfenol-D/Metglas magnetoelectric laminate composites, J. Appl. Phys. **107**, 094109 (2010).

[51] V. Annapureddy, S.-M. Na, G.-T. Hwang, M. G. Kang, R. Sriramdas, H. Palneedi, W.-H. Yoon, B.-D. Hahn, J.-W. Kim, C.-W. Ahn, D.-S. Park, J.-J. Choi, D.-Y. Jeong, A. B. Flatau, M. Peddigari, S. Priya, K.-H. Kim, and J. Ryu, Exceeding milli-watt powering magneto-mechano-electric generator for standalone-powered electronics, Energy Environ. Sci. **11**, 818 (2018).

[52] Z. Chu, V. Annapureddy, M. PourhosseiniAsl, H. Palneedi, J. Ryu, and S. Dong, Dual-stimulus magnetoelectric energy harvesting, MRS Bull. **43**, 199 (2018).

[53] A. E. Clark, J. B. Restorff, M. Wun-Fogle, T. A. Lograsso, and D. L. Schlagel, Magnetostrictive properties of body-centered cubic Fe-Ga and Fe-Ga-Al alloys, IEEE Trans. Magn. **36**, 3238 (2000).

[54] J. Atulasimha and A. B. Flatau, A review of magnetostrictive iron–gallium alloys, Smart Mater. Struct. **20**, 043001 (2011).

[55] W. Jahjah, R. Manach, Y. Le Grand, A. Fessant, B. Warot-Fonrose, A. Prinsloo, C. Sheppard, D. Dekadjevi, D. Spenato, and J.-P. Jay, Thickness Dependence of Magnetization Reversal and Magnetostriction in Fe_81Ga_19 Thin Films, Phys. Rev. Appl. **12**, 024020 (2019).

[56] P. Finkel, R. Pérez Moyet, M. Wun-Fogle, J. Restorff, J. Kosior, M. Staruch, J. Stace, and A. Amin, Nonresonant magnetoelectric energy harvesting utilizing phase transformation in relaxor ferroelectric single crystals, Actuators **5**, 2 (2015).

[57] L. Wang, Z. Du, C. Fan, L. Xu, H. Zhang, and D. Zhao, Magnetoelectric properties of Fe-Ga/$BaTiO_3$ laminate composites, J. Alloys Compd. **509**, 508 (2011).

[58] S. Dong, J. Zhai, N. Wang, F. Bai, J. Li, D. Viehland, and T. A. Lograsso, Fe-Ga/$Pb(Mg_{1/3}Nb_{2/3})O_3$-$PbTiO_3$ magnetoelectric laminate composites, Appl. Phys. Lett. **87**, 222504 (2005).

[59] D. E. Parkes, S. A. Cavill, A. T. Hindmarch, P. Wadley, F. McGee, C. R. Staddon, K. W. Edmonds, R. P. Campion, B. L. Gallagher, and A. W. Rushforth, Non-volatile voltage control of magnetization and magnetic domain walls in magnetostrictive epitaxial thin films, Appl. Phys. Lett. **101**, 072402 (2012).

[60] Y. Xie, Q. Zhan, Y. Liu, G. Dai, H. Yang, Z. Zuo, B. Chen, B. Wang, Y. Zhang, X. Rong, and R.-W. Li, Electric-field control of magnetic anisotropy in $Fe_{81}Ga_{19}$/$BaTiO_3$ heterostructure films, AIP Adv. **4**, 117113 (2014).

[61] M. Liu and N. X. Sun, Voltage control of magnetism in multiferroic heterostructures, Philos. Trans. R. Soc. A: Math., Phys. Eng. Sci. **372**, 20120439 (2014).

[62] H. Ahmad, J. Atulasimha, and S. Bandyopadhyay, Electric field control of magnetic states in isolated and dipole-coupled FeGa nanomagnets delineated on a PMN-PT substrate, Nanotechnology **26**, 401001 (2015).

[63] N. N. Phuoc and C. K. Ong, Electrical manipulation of electromagnetic properties of FeGa/[$Pb(Mg_{1/3}Nb_{2/3})O_3$] 0.68–[$PbTiO_3$]0.32(011) multiferroic heterostructures, J. Mater. Sci.: Mater. Electron. **28**, 5628 (2017).

[64] Y. Zhang, C. Huang, M. Turghun, Z. Duan, F. Wang, and W. Shi, Electric-regulated enhanced in-plane uniaxial anisotropy in FeGa/PMN–PT composite using oblique pulsed laser deposition, Appl. Phys. A **124**, 289 (2018).

[65] Z. Hu, T. Nan, X. Wang, M. Staruch, Y. Gao, P. Finkel, and N. X. Sun, Voltage control of magnetism in FeGaB/PIN-PMN-PT multiferroic heterostructures for high-power and high-temperature applications, Appl. Phys. Lett. **106**, 022901 (2015).

[66] J. Lou, M. Liu, D. Reed, Y. Ren, and N. X. Sun, Giant electric field tuning of magnetism in novel multiferroic FeGaB/Lead zinc niobate-lead titanate (PZN-PT) heterostructures, Adv. Mater. **21**, 4711 (2009).

[67] J. Zhang, P. Li, Y. Wen, W. He, A. Yang, D. Wang, C. Yang, and C. Lu, Giant self-biased converse magnetoelectric effect in multiferroic heterostructure with single-phase magnetostrictive materials, Appl. Phys. Lett. **105**, 172408 (2014).

[68] S. Chul Yang, K.-H. Cho, C.-S. Park, and S. Priya, Self-biased converse magnetoelectric effect, Appl. Phys. Lett. **99**, 202904 (2011).

[69] T. Fitchorov, Y. Chen, L. Jiang, G. Zhang, Z. Zhao, C. Vittoria, and V. G. Harris, Converse magnetoelectric effect in a Fe-Ga/PMN-PT laminated multiferroic heterostructure for field generator applications, IEEE Trans. Magn. **47**, 4050 (2011).

[70] S. K. Mandal, G. Sreenivasulu, V. M. Petrov, and G. Srinivasan, Magnetization-graded multiferroic composite and magnetoelectric effects at zero bias, Phys. Rev. B **84**, 014432 (2011).

[71] Y. Zhou, D. Maurya, Y. Yan, G. Srinivasan, E. Quandt, and S. Priya, Self-biased magnetoelectric composites: An overview and future perspectives, Energy Harvesting Syst. **3**, 1 (2016).

[72] M. Fiebig, T. Lottermoser, D. Meier, and M. Trassin, The evolution of multiferroics, Nat. Rev. Mater. **1**, 16046 (2016).

[73] Ceracomp Co. Ltd., Korea, http://www.ceracomp.com

[74] M. Shanthi, L. C. Lim, K. K. Rajan, and J. Jin, Complete sets of elastic properties of flux-grown [011]-poled $Pb(Mg_{1/3}Nb_{2/3})O_3$–(28–32)% $PbTiO_3$ single crystals, dielectric, and piezoelectric, Appl. Phys. Lett. **92**, 142906 (2008).

[75] Schott D 263 TM Glass, https://www.schott.com/nextertion/english/products/uncoated-substrates/d263.html?highlighted˙text=d263

[76] Evico Magnetics, Dresden, http://www.evico-magnetics.de

[77] Cryogenic Ltd., London, UK, Cryogen free magnet system user manual (2016).

[78] P. Zhao, M. Bao, A. Bur, J. L. Hockel, K. Wong, K. P. Mohanchandra, C. S. Lynch, and G. P. Carman, Domain engineered switchable strain states in ferroelectric (011) $[Pb(Mg_{1/3}Nb_{2/3})O_3]_{(1-x)} - [PbTiO_3]_x$ (PMN-PT, $x \approx 0.32$) single crystals, J. Appl. Phys. **109**, 124101 (2011).

[79] W. Huang, S. Yang, and X. Li, Multiferroic heterostructures and tunneling junctions, J. Materiomics **1**, 263 (2015).

[80] S. Zhang *et al.*, Electric-Field Control of Nonvolatile Magnetization in $Co_{40}Fe_{40}B_{20}/Pb(Mg_{1/3}Nb_{2/3})_{0.7}Ti_{0.3}O_3$ Structure at Room Temperature, Phys. Rev. Lett. **108**, 137203 (2012).

[81] L. Yang, Y. Zhao, S. Zhang, P. Li, Y. Gao, Y. Yang, H. Huang, P. Miao, Y. Liu, A. Chen, C. W. Nan, and C. Gao, Bipolar loop-like non-volatile strain in the (001)-oriented $Pb(Mg_{1/3}Nb_{2/3})O_3$-$PbTiO_3$ single crystals, Sci. Rep. **4**, 4591 (2015).

[82] Y. Wei, C. Gao, Z. Chen, S. Xi, W. Shao, P. Zhang, G. Chen, and J. Li, Four-state memory based on a giant and non-volatile converse magnetoelectric effect in FeAl/PIN-PMN-PT structure, Sci. Rep. **6**, 30002 (2016).

[83] J. Wang, D. Pesquera, R. Mansell, S. van Dijken, R. P. Cowburn, M. Ghidini, and N. D. Mathur, Giant non-volatile magnetoelectric effects via growth anisotropy in $Co_{40}Fe_{40}B_{20}$ films on PMN-PT substrates, Appl. Phys. Lett. **114**, 092401 (2019).

[84] C. Jiang, C. Zhang, C. Dong, D. Guo, and D. Xue, Electric field tuning of non-volatile three-state magnetoelectric memory in FeCo-$NiFe_2O_4/Pb(Mg_{1/3}Nb_{2/3})_{0.7}Ti_{0.3}O_3$ heterostructures, Appl. Phys. Lett. **106**, 122406 (2015).

[85] D. Damjanovic, in *Science of Hysteresis* (Academic Press, 2006), p. 337.

[86] X. Guo, X. Han, Y. Zuo, J. Zhang, D. Li, B. Cui, K. Wu, J. Yun, T. Wang, Y. Peng, and L. Xi, Electric field induced magnetic anisotropy transition from fourfold to twofold symmetry in (001) $0.68Pb(Mg_{1/3}Nb_{2/3})O_3 - 0.32PbTiO_3/Fe_{0.86}Si_{0.14}$ epitaxial heterostructures, Appl. Phys. Lett. **108**, 152401 (2016).

[87] Y. Chen, A. L. Geiler, T. Fitchorov, C. Vittoria, and V. G. Harris, Time domain analyses of the converse magnetoelectric effect in a multiferroic metallic glass-relaxor ferroelectric heterostructure, Appl. Phys. Lett. **95**, 182501 (2009).

[88] D. C. Lupascu and C. Verdier, Fatigue anisotropy in lead-zirconate-titanate, J. Eur. Ceram. Soc. **24**, 1663 (2004), electroceramics VIII.

[89] V. Gopalan and M. C. Gupta, Observation of internal field in $LiTaO_3$ single crystals: Its origin and time-temperature dependence, Appl. Phys. Lett. **68**, 888 (1996).

[90] Y. Noguchi, I. Miwa, Y. Goshima, and M. Miyayama, Defect control for large remanent polarization in bismuth titanate ferroelectrics—doping effect of higher-valent cations—, Jpn. J. Appl. Phys. **39**, L1259 (2000).

[91] J. Cullen, P. Zhao, and M. Wuttig, Anisotropy of crystalline ferromagnets with defects, J. Appl. Phys. **101**, 123922 (2007).

[92] A. Begué, M. G. Proietti, J. I. Arnaudas, and M. Ciria, Magnetic ripple domain structure in FeGa/MgO thin films, J. Magn. Magn. Mater. **498**, 166135 (2019).

[93] R. O. Cherifi, V. Ivanovskaya, L. C. Phillips, A. Zobelli, I. C. Infante, E. Jacquet, V. Garcia, S. Fusil, P. R. Briddon, N. Guiblin, A. Mougin, A. A. Ünal, F. Kronast, S. Valencia, B. Dkhil, A. Barthélémy, and M. Bibes, Electric-field control of magnetic order above room temperature, Nat. Mater. **13**, 345 (2014).

[94] J. T. Heron, J. L. Bosse, Q. He, Y. Gao, M. Trassin, L. Ye, J. D. Clarkson, C. Wang, J. Liu, S. Salahuddin, D. C. Ralph, D. G. Schlom, J. Iñiguez, B. D. Huey, and R. Ramesh, Deterministic switching of ferromagnetism at room temperature using an electric field, Nature **516**, 370 (2014).

[95] G. Wu, R. Zhang, and N. Zhang, Enhanced converse magnetoelectric effect in cylindrical piezoelectric-magnetostrictive composites, Eur. Phys. J. Appl. Phys. **76**, 10602 (2016).

[96] J. Han, J. Zhang, and Y. Gao, A nonlinear magneto-mechanical-thermal-electric coupling model of terfenol-D/PZT/Terfenol-D and Ni/PZT/Ni laminates, J. Magn. Magn. Mater. **466**, 200 (2018).

[97] D. A. Burdin, Y. K. Fetisov, D. V. Chashin, and N. A. Ekonomov, Temperature dependence of the characteristics of the resonant magnetoelectric effect in a lead magnesium niobate-lead titanate/nickel structure, Tech. Phys. Lett. **38**, 661 (2012).

[98] Y. Zhang, Q. Zhan, X. Rong, H. Li, Z. Zuo, Y. Liu, B. Wang, and R.-W. Li, Influence of thermal deformation on exchange bias in FeGa/IrMn bilayers grown on flexible polyvinylidene fluoride membranes, IEEE Trans. Magn. **52**, 1 (2016).

[99] Y. Liu, B. Wang, Q. Zhan, Z. Tang, H. Yang, G. Liu, Z. Zuo, X. Zhang, Y. Xie, X. Zhu, B. Chen, J. Wang, and R.-W. Li, Positive temperature coefficient of magnetic anisotropy in polyvinylidene fluoride (PVDF)-based magnetic composites, Sci. Rep. **4**, 6615 (2015).

[100] Y. Liu, Q. Zhan, G. Dai, X. Zhang, B. Wang, G. Liu, Z. Zuo, X. Rong, H. Yang, X. Zhu, Y. Xie, B. Chen, and R.-W. Li, Thermally assisted electric field control of magnetism in flexible multiferroic heterostructures, Sci. Rep. **4**, 6925 (2015).